Exploring the potential relationship between the occurrence of debris flow and landslide

Zhu Liang[1], Changming Wang[1], Donghe Ma[2] and Kaleem Ullah Jan Khan[1]

[1]College of Construction Engineering, Jilin University, 130000 Changchun, People's Republic of China;

[2]China Water Northeastern Investigation, Design and Research Co.Ltd.

E-mail:wangcm@jlu.edu.cn

Abstract: The present study is to explore the potential relationship between debris flow and landslide by establishing susceptibility zoning maps (SZM) separately with the use of random forest (RF). Longzi County, located in Southeastern Tibet, was selected as the study area. The work has been carried out with the following steps: **(1)** An inventory map consisting of 399 landslides and 49 debris flows was determined; **(2)** Slope units and 11 conditioning factors were prepared for the susceptibility modelling of landslide while watershed units and 12 factors for debris flow; **(3)** SZM were constructed for landslide and debris flow, respectively, with the use of RF; **(4)** The performance of two models were evaluated by 5-fold cross-validation using receiver operating characteristic (ROC), area under the curve (AUC) and statistical measures; **(5)** The potential relationship between landslide and debris flow was explored by the superimposition of two zoning maps; **(6)** Gini index was applied to determined the major factors and analyze the difference between debris flow and landslide; **(7)** A combined susceptibility map with two considered hazardous phenomena was obtained. Two used models had demonstrated great

predictive capabilities, of which accuracy and AUC was 87.33% and 85.17%, 0.902 and 0.892, respectively. Comparing the overlap of different susceptibility classes for two obtained maps, it concluded that there is no straightfoward relationship between the occurrence of debris flow and landslide. Although most landslides can be converted into debris flow, the area prone to debris flow did not promote the occurrence of landslide. A susceptibility zoning map composed of two or more hazardous phenomena is comprehensive and significant in this regard, which provides valuable reference for researches of disaster-chain and engineering applications.

Key words: Landslide; Debris flow; Susceptibility; Random forest; Potential relationship

1. Introduction

Soil slide and debris flow are two kinds of natural phenomenon mainly occurring in mountainous areas, which pose considerable threats to people, industries, and the environment directly or indirectly. Generally, damages can be decreased to a certain extent by predicting the likely location of future disasters (Pradhan, 2010). Thus, extensive research has been conducted for the prediction and susceptibility assessment of landslide and debris flow.

In geomorphology, a "landslide" is the movement of a mass of rock, debris or earth down a slope, under the influence of gravity (Cruden and Varnes, 1996). According to different variables, landslides can be divided into different types (Varnes, 1978). Debris flow is a specific type of landslide, which can be defined as (Hungr et al. 2013): ''Very rapid to extremely rapid surging flow of saturated debris in a steep channel". Most of debris flows are runoff generated (Imaizumi et al., 2006; Ma et al., 2018; Theule et al., 2020). Generally, landslide that occur on a steep slope

and become disaggregated as they tumble down can transform into debris flows if they contain sufficient water for saturation (Huang et al., 2020). Debris flow usually occurs on a channel bed for the entrainment into abundant runoff of debris supplied by deep or shallow slides of slopes incised by the channel (Hurlimann et al., 2014; Imaizumi et al.2019; Zhou et al., 2019; Simoni et al., 2020). Therefore, landslides may provide sufficient material source for debris flow and most of the landslides are accompanied by debris flow (Iverson et al., 1997; Lan et al., 2004). The conditioning factors and mapping units involved in the susceptibility assessment for different kinds of landslides are not identical. In the past, some scholars made separate evaluations between landslide and debris flow (Park et al., 2011; Haydar et al., 2016). Some scholars have explored the mobilization of debris flow from landslide and the material source of the debris flow is not necessary coming from landslides (Chiang et al., 2012; Gomes et al., 2013). Besides, the formation and manifestations of landslides and debris flow are different (Varnes, 1978). In other words, there is no determined connection between debris flow and landslide. However, seldom researches have explored the potential relationship between debris flow and landslide through the separated susceptibility maps (Alessandro et al., 2015).

The methods used for the susceptibility assessment can be broadly classified as qualitative or quantitative (Aleotti et al., 1999). About the quantitative methods there are those physically-based (Carrara et al., 2008), those heuristic (Blais et al., 2016) and those statistically-based (Reichenbach et al., 2018). Recently new machine learning models have been used for susceptibility analysis: neural networks (Park et al.,2013), support vector machines (Colkesen et al.,2016) and random forest (RF) (Zhu et al., 2020a).

The present study is to explore the potential relationship between the occurrence of debris

flow and landslide by establishing susceptibility zoning maps separately with the use of RF. The Longzi County in Southeastern Tibet is exposed to landslide and debris flow and chosen as the study area.

2. Materials

2.1 Study area

The study area located in Longzi Township, Longzi County, Southeastern Tibet is bounded by longitudes of 92°15'E and 92°45'E, latitudes of 28°10'N and 28°30'N (Fig.1). It covers a surface of about 535 km^2 with a population of more than 6000. It belongs to a semi-arid temperate monsoon climate with the annual rainfall of 279 mm, mainly concentrated in May to September. The seismic intensity within the area has a degree of VIII on the modified Mercalli index.

The study area is distributed in the zone of stratigraphic division of the Northern Himalayan block. The strata is mainly composed of Mesozoic Cretaceous, Jurassic, Triassic, and Cenozoic units. Three types of lithology were mainly observed during our field investigation: Siltstone from the Laka Formation (K_1l); Conglomerates from the Weimei Formation (J_3w) and Quaternary slope wash (Q_4^{el+dl}) from the Cenozoic strata.

Main disasters in the study area consist of rain-fed high frequency debris flows and landslides, which destroyed and flooded roads, bridges, farmlands, villages, etc., causing great economic losses.

2.2 Landslide and debris flow inventory

The statistically-based susceptibility models are based on an important assumption: future

85 landslides have more chances to occur again under the conditions which led to the landslides past
86 and present (Varnes, 1984). Therefore, a complete inventory map is the key for modeling. In this
87 study, data comes from historical records (1970~2010), field surveys from 2000~2003 (**Fig.2 and**
88 **Fig.3**) and interpretation of Google Earth images carried out in Google Earth pro 7.1 (**Fig.4**).
89 Finally, a total of 399 landslides and 49 debris flow locations with positive label were recorded
90 and mapped as a point (**Fig.1**) and the same number of non-landslide points with negative were
91 selected randomly from the landslide-free area.

92 2.3 Mapping units

93 The selection of the mapping unit is an important pre-requisite for modelling (Guzzetti, 2006a).
94 The mapping units commonly used are grid cells (Reichenbach et al., 2018). Despite its popularity
95 and operational advantages, grid-cells have clear drawbacks (Guzzetti et al., 1999). There is no
96 physical relationship between a grid-cell or a group of grid-cells and slope, while slope units can
97 make up for this deficiency (Reichenbach et al., 2018). A slope unit may correspond to an
98 individual slope, an ensemble of adjacent slopes or a small catchment. The geometry of the debris
99 flow is tortuous and complex, which is not suitable to represent it with a regular grid unit. In the
100 present study, adjacent slope units were applied to the modeling. First-order sub-catchments,
101 which are also called watershed unit, were applied to the susceptibility of debris flow (Bregoli et
102 al., 2015; Zhu et al., 2020b). Accordingly, the study area was divided into 1003 slope units for the
103 modeling of landslide or 174 watershed units for debris flow.

104 2.4 Controlling factors and mapping

105 The selection of evaluation parameters is another key prerequisite to ensure that the model is

106 accurate. Different researches emphasized different controlling factors but availability, reliability,
107 and practicality of the data were first considered (van Westen et al., 2008; Ahmed et al., 2016;
108 Braun et al., 2018). In this paper, 11 controlling factors are selected for landslide susceptibility
109 assessment and 12 for debris flow. A brief description of each controlling factor is given below.
110 Detailed information is shown in **Fig.5a~5m**.

111 2.4.1 Factors used in landslide susceptibility assessment

112 Aspect reflects sunshine duration and rainfall, which is frequently used as landslide
113 controlling factor (Dai and Lee, 2002) and was reclassified into 8 classes (**Fig. 5g**). Plan curvature
114 and profile curvature which reflect the relief of the terrain were both considered and reclassified
115 into six classes (**Fig. 5b and 5e**). Generally, faults, rivers and roads play a key role in the
116 occurrence of landslides as landslides are more likely disturbed around faults, rivers and roads
117 (Taskin et al., 2015) which were reclassified into seven classes using an interval of 1500m (**Fig.**
118 **5i~k**). Topographic wetness index (TWI) belong to a hydrological variable that reflects both slope
119 and soil moisture content (Wilson and Gallant 2000) and was reclassified into five classes (**Fig.**
120 **5h**).

121 2.4.2 Factors used in debris flow susceptibility assessment

122 Pre-even normalized difference vegetation index (NDVI) reflects the vegetation conditions
123 in the area and was reclassified into 5 classes (**Fig. 6b**). Drainage density is the ratio of the total
124 drainage length to the watershed area and was reclassified into six classes (**Fig.6 g**). Roundness
125 refers to the ratio of the area of a basin to the area of a circle with the same circumference and was
126 reclassified into six classes (**Fig.6 d**). Melton ratio refers to the ratio of the degree of undulation in

the watershed to the square root of the arithmetic area of the watershed (Melton, 1965), which is reclassified into seven classes (**Fig. 6a**). Basin area and main channel length are represented by the same graph and was reclassified into four classes (**Fig.6h**). Average gradient of main channel, which is the ratio of the maximum elevation difference of main channel to its linear length, was reclassified into six classes (**Fig. 6j**).

2.4.3 Factors used in both landslide and debris flow

Rainfall is the only triggering factor to be considered for both landslide and debris flow in this paper, which was reclassified into six classes (**Fig. 5a and Fig. 6c**). Slope angle which reflects kinetic energy conditions is frequently employed in both landslide and debris flow susceptibility mapping and was reclassified into six classes (**Fig. 5f and Fig. 6i**). Maximum elevation difference also reflects the kinetic energy condition and is reclassified into 6 classes using an interval of 200m (**Fig. 5c and Fig. 6e**). Elevation affects the rainfall and vegetation (**Fig. 5d and Fig. 6f**) and was reclassified into five classes in the study (Pourghasemi et al. 2013a, b).

The values of controlling factors were classified by processing the raw data in the ArcGIS 10.2 platform. Morpholigical and topographic related factors were derived from the DEM with a resolution of 30 × 30 m (http://www.gscloud.cn). Geological related factors were extracted from 1:50000 geological maps (http://www.ngac.org.cn/). Rainfall is one of the most important external factors inducing landslides and debris flow, which was determined by ordinary kriging interpolation in ArcGIS based on 11 precipitation stations data near the study area collected from the China Meteorological Administration. Roads networks are provided by Landsat 8 LOI images (2018.8.12).

3. Methods

3.1 Sampling strategy and performance assessment

Statistical models for landslide susceptibility zoning reconstruct the relationships between dependent and independent variables using training data set, and verify these relationships using validation sets (Guzzetti et al., 2006b), which usually implies the partitioning of the inventory in subsets. The sampling strategy affects the results of the susceptibility map (Yilmaz, 2010). The partition of landslide inventory is approached based on temporal, spatial or random criteria, (Chung and Fabbri, 2003) and among them that of one time random selection is the most used. However, there is a need for a more reliable estimation of the model performance. The ability of the models to classify independent test data was elaborated using a 5-fold cross validation procedure (James et al., 2013).

The value of AUC is the most popular metrics to estimate the quality of model, which has been applied for ROC curves (Green and Swets, 1966). Three extra statistical metrics as accuracy, sensitivity, and specificity are combined to assess the performance of models (Tien Bui et al. 2016).

$$Accuracy = \frac{TP + TN}{TP + TN + FP + FN}$$

$$Sensitivity = \frac{TP}{TP + FN}$$

$$Specificity = \frac{TN}{FP + TN} \quad (1)$$

where True Positives (*TP*), i.e., cells predicted unstable and observed unstable, True Negatives (*TN*), i.e., cells predicted stable and observed stable, False Positives (*FP*), i.e., cells predicted

168 unstable but observed stable and False Negatives (*FN*), i.e., cells predicted stable but observed
169 unstable.

170 3.2 Random Forests

171 RF is a powerful ensemble-learning method and was first introduced by Breiman (2001). Bagging
172 technique is applied to select random samples of variables and observations as the training data set
173 at each node of the tree for the modeling of RF. Unselected cases (out of bag) are used to calculate
174 the error of the model (OOB Error). The increase in OOB error is proportional to the importance
175 of the predictive variable (Breiman and Cutler 2004). There are no restrictions on the types of
176 variables, either numerical or categorical. RF has the ability to reduce errors caused by unbalanced
177 data, which is suitable for susceptibility assessment.

178 The number of trees and the number of predictive variables used to split the nodes are two
179 user-defined parameters (Ahmed et al.,2016). Cross-Validation were applied to optimized the
180 hyper-parameters before application (Schratz et al., 2019). Scikit-learn package (Pedregosa et al.,
181 2011) in the programming software python version 3.7 was used for the modeling. Gini index (the
182 larger the value of the obtained result, the greater the contribution to the occurrence of landslide)
183 (Breiman, 2001) was applied to analyze the relative importance of conditioning factors.

184 4. Results and verification

185 4.1 Landslide susceptibility mapping results

186 The predictive accuracy, ROC curves and AUC values of the RF models using training data set
187 were showed in **Table 1** and **Fig. 7**. The RF model ensured a satisfactory performance for

188 classifying landslides with a sensitivity value of 91.62%. In terms of the classification of
189 non-landslides zones, specificity value also reached 89.06%. An AUC value ranges from 0.5 to 1
190 and equals to 1 indicates perfect prediction accuracy (Vorpahl et al., 2012). The RF model had
191 great performance in terms of AUC, with a value of 0.976. Standard error (St.), confidence
192 interval (CI) at 95% and significance (Sig.) were applied as three evaluation statistics. All these
193 results indicated that the models achieved a reasonable goodness-of-fit, for which the values were
194 reasonably small.

195 Verifying the generalization ability of the model is a key step in prediction models as shown
196 in **Table 2** and **Fig. 7**. Accordingly, the values of sensitivity and specificity were 88.69% and
197 86.05%, respectively. The model also achieved a great performance in terms of AUC with a value
198 of 0.902. In comparison with the training dataset, the accuracy and AUC values have slightly
199 decreased, but still perform well.

200 The landslide susceptibility map was reclassified into five classes: very low (0~0.2), low
201 (0.2~0.4), moderate (0.4~0.6), high (0.6~0.8), very high (0.8~1) by using the equal spacing
202 method (**Fig.8**). The map should satisfy two spatial effective rules: (1) The existing disaster points
203 should belong to the high-susceptibility class and **(2)** The high-susceptibility class should cover
204 only small areas (Bui et al. 2012). The number of units belonging to very high class accounted for
205 17% of the total number of units (**Fig.9**). Disaster points were mostly in the dark (red or orange)
206 areas. The units belonging to moderate class accounted for the smallest proportion, at 13% of the
207 total number of units (**Fig.9**).

208 The controlling factors with significant effects were selected and normalized as shown in
209 **Table 3**. The weight values of slope angle, distance to fault, plan curvature and topographic wetness

index were 0.21, 0.19, 0.17, 0.13 respectively, which was closely related to the occurrence of landslide. The weight values of distance to road, maximum elevation difference, profile curvature and elevation are less than 0.1 as 0.08, 0.08, 0.06, and 0.05, respectively (**Fig.10**).

4.2 Debris flow susceptibility mapping result

The debris flow susceptibility model perform well with a very high sensitivity and specificity values as 87.80% and 88.89%, respectively. In terms of accuracy and AUC, the model had also a great prediction performance with the value of 88.57% and 0.967 (**Fig.7**). Three evaluation statistics also indicate a reasonable goodness-of-fit for the model.

Table 2 shows that the values of sensitivity and specificity were 85.71% and 84.62%, which were slightly decreased compared to the training model. However, the model had achieved a great performance in terms of AUC, with value of 0.892.

The number of units belonging to very high-class accounted for 15% of the total number of units while the units belonging to high-class accounted for the smallest proportion at 13%. More than half of the units (58%) belong to on a low or very low-class (**Fig.9**). Disaster points were mostly in the dark (Bright or deep red) areas (**Fig.8**).

The weight values of main channel length, roundness and slope angle were 0.25, 0.16, 0.14 respectively and these factors have significant influence on the occurrence of debris flow (**Table 4**). The weight values of elevation, maximum elevation difference, melton ratio and basin area are close to 0.1, which are 0.13, 0.12, 0.1, and 0.1 respectively (**Fig.10**).

4.3 Analysis and comparison of landslide and debris flow susceptibility

It is worth comparing the two susceptibility zoning maps. In terms of prediction accuracy, the values of sensitivity, specificity and AUC of landslide model were slightly higher than that of debris flow. However, both models achieved high predictive performance. Therefore, the landslide and debris flow susceptibility assessment models based on RF are reliable. The purpose of the present study is to explore the potential relationship between landslides and debris flows by establishing the respective susceptibility zoning maps. Figure 11 shows the overlapping areas between debris flow and landslide in high or very high-class of susceptibility zoning map. It can be seen that most of the areas with high or very high-class in the map of debris flow are covered with landslides. However, there are also non-overlapping areas between the two zoning maps. There are 23 watershed units belonging to high-class in the debris flow susceptibility zoning map (**Fig.8**), of which 17 units correspond to high or very high-class slope units in the landslide zoning map (**Table 5**). In addition, there are 4 watershed units covered with low or very low class slope units. In the same way, 19 watershed units belonging to very high-class are covered with high or very high-class slop units and 4 watershed units with low or very low-class slop units. In other words, more than 70% of the high or very high-class watershed units are covered with high or very high-class slope units. However, there are still 30% of watershed units with high or very high-class without the distribution of slope units in corresponding grades. It validated the previous view that most of landslides can be transformed into debris flows.

Factor analysis which is a tool for dimensionality reduction and exploring the major factors was applied to further analyze the reasons for the difference (Zhu et al., 2020a). 36 watershed

251 units with distribution of high or very high-grade slope units were taken as model 1 and the left 8
252 watershed units as model 2 . The KMO (Kaiser-Meyer-Olkin) and Sig. testing are two statistical
253 parameters which ensured the feasibility before application, which are provided by SPSS
254 (Statistical Product and Service Solutions). The closer the KMO statistic is to 1, the stronger the
255 correlation between variables and the better the effect of factor analysis. The KMO values were
256 0.766 and 0.643 respectively, which indicated that the correlation between variables was obvious
257 and suitable for factor analysis (**Table 6)**. In model 1, the cumulative contribution rate of the first
258 three factors (C1, C2 ,C3) reached to 83.6%, while the cumulative contribution rate of the first
259 four factors (F1, F2 ,F3 and F4) reached to 80.5% for model 2 (**Table 7**). According to the
260 correlation coefficient of each common factor, the first common factor mainly highlighted the
261 information of basin area, main channel length and maximum elevation difference. Similarly, the
262 second and the third common factor highlighted the information of slope angle and elevation and
263 roundness, respectively. The difference between the two models (model 1 and model 2) is that the
264 second model has the fourth common factor (**Table 8**), which emphasized the effects of rainfall
265 and distance to the fault. The transformation from a landslide to a debris flow often occurs during
266 heavy rainfall (Takahashi, 1978), and the landslides are the source area. But landslides are not the
267 only source of debris flows. The loose material distributed in the basin is not necessarily caused
268 by landslide.

269 In turn, we analyze the distribution of high or very high-class slope units in watershed units.
270 The landslide zoning map was put at the bottom floor and the debris flow zoning map on the top
271 floor (**Fig. 11**). There are 167 slope units belonging to high-class, of which 68 units (accounting
272 for about 40%) are distributed in the area of high or very high-class watershed units in the debris

flow zoning map (**Table 9**). Besides, 69 slope units (accounting for about 41%) are distributed in the area of low or very low-class watershed units. Similarly, 53 slope units (accounting for about 30%) belonging to very high-class are distributed in the area of high or very high-class watershed units and 88 slope units (accounting for about 50%) in low or very low-class slop units (**Table 9**). Comparing with the extent of the landslide affecting the debris flow, the impact of the debris flow on the landslide is not obvious. It indicated that the area prone to debris flow does not promote the occurrence of landslides.

Finally, we took the center of gravity of 1,003 slope units as the potential hazard points and spread them over 174 watershed units. Thus, a combining susceptibility zonation map for landslide and debris flow was obtained (**Fig.11**). The darker the color, the higher the class of susceptibility will be. It can be seen that the susceptibility in the south is generally higher than that in the north, and the area in the southwest is disaster-prone. The northeast and central locations in the area are less likely to be affected by landslides and belong to low-susceptibility areas. Green or yellow dots, which refer to slope units with very low or low- class in the landslide zoning map, mainly distributed in light-colored areas but there are also quite a few green or yellow dots distributed in dark areas, which means that the occurrence of debris flow not necessarily depend on landslides. Blue or black spots are mainly distributed in dark areas but there are also quite a few blue or black spots distributed in dark light areas, which means that landslide is not the only condition for debris flow to occur. Most of the watershed units are distributed with two or more colored dots, which means that there would be multiple slope units with different susceptibility class in the same watershed. According to the combining susceptibility zoning map of landslide and debris flow, the study area can be divided into 4 categories: **(1)** Low or very low-class

watershed units coupled with low or very low-class slope units; **(2)** Low or very low-class watershed units coupled with high or very high-class slope units; **(3)** High or very high-class watershed units coupled with low or very low-class slope units; **(4)** High or very high-class watershed units coupled with high or very high-class slope units. We assume that the occurrence of landslides can bring rich sources of debris flow, thereby promoting or aggravating the outbreak of debris flow, that is, forming a landslide-debris flow disaster chain. Therefore, the susceptibility assessment of the landslide-debris flow chain in the study area can be roughly divided into three classes, which are low, moderate and high (**Table 10**).

5.Discussion

5.1 Method used for modeling

Many researchers have used different statistically-based methods to evaluate the susceptibility of landslides or debris flows. Logistic regression and discriminant analysis are the most popular methods to use in traditional multivariate statistical analysis (Teigila, 2015; Abdelaziz et al., 2020). The performance of new learning machines, such as support vector machines and neural networks, has also been verified. RF has been little used until now for susceptibility analysis of landslide and debris flows (Chen et al., 2017; Zhang et al., 2017). Actually, RF have powerful data processing capabilities and can simultaneously solve problems such as high-dimensional, unbalanced and data loss, which are common in geological disaster assessment. Most importantly, RF can compare the important differences between features and have ability to reduce errors caused by unbalanced data and, which achieved strong generalization properties (Zhu et al., 2020a, c).

5.2 Potential relationship between landslide and debris flow

There is a certain similarity in the evaluation of the susceptibility of landslide and debris flow as the selection of controlling factors and the application of modeling strategies. Therefore, some researchers have neglected the difference between landslide and debris flow i.e to express two different disasters with the same susceptibility zoning map (Mariantonietta et al., 2017; Persichillo et al., 2017). However, similarity does not always mean consistency. Many researchers have previously conducted studies into the debris flow mobilization from shallow landslide using a coupled methodology (Wang et al., 2013; Fan et al., 2017). However, not every landslide evolves into a debris flow, which means that the analysis process is highly selective or uncertain. In the

same way, the source of the debris flow is not limited to landslide. There, the potential relationship between landslide and debris flow needs to be discussed more reasonably and effectively. In this study, the corresponding influencing factors and mapping units are selected to establish landslide and debris flow susceptibility zoning maps, respectively. The potential relationship between landslide and debris flow is explored in two ways: **1)** Superimposing the high or very high-class susceptibility areas in the two maps; **2)** Transforming the slope units into points and distributed them on the watershed units. The relationship between landslide and debris flow is illustrated by the distribution of slope units of different grades on the watershed units with different prone grades. Different kinds of landslides should be evaluated respectively conditioning that conditioning factors and scale varies.

5.3 Necessity and feasibility of combining multiple natural disaster susceptibility zoning maps

Previous studies on susceptibility zoning mapping of disaster have agreed that one disaster corresponds to one map. However, it will cause some confusion in practical. For example, multiple disasters may be bred simultaneously in a watershed unit. For another case, the probability of one kind of disaster like debris flow in a watershed is negligible, while another disaster like rockfall occurs frequently. Therefore, we need to combine multiple zoning maps at the same time to give a comprehensive evaluation, which is arduous to achieve. On the one hand, the prediction accuracy and error of different zoning maps should be similar or even consistent. On the other hand, the dimensions of the mapping unit should be consistent or complementary. The fact that the appropriate prediction method (like RF applied in this study) and mapping units

applied to the two disasters makes it possible to merge the two zoning maps. Disaster risk is higher in landslide-debris flow chain, causing significant loss of life and property. Therefore, two natural disasters with potential relationship are simultaneously reflected in the same susceptibility zoning map, which can better guide the implementation of engineering, such as landslide-debris flow disaster chain.

5. Conclusion

In this study, susceptibility assessment models for landslide and debris flow are established through RF, respectively and the performance of the models are excellent in terms of accuracy and goodness of fit. The potential relationship between landslide and debris flow is discussed by the superimposition of two zoning maps and the following conclusions can be drawn:

(1) The landslide and debris flow susceptibility mapping based on RF models have great performance of accuracy and goodness-of-fit and have the ability to analyze the relative importance of different impact factors, which is suitable for the evaluation of natural disasters;

(2) There is no straightfoward relationship between the occurrence of the two considered phenomena. Although most landslides will be converted into debris flow, the landslides are not necessarily the source of debris flow, and the loose sources carried by the debris flow are not necessarily brought by the landslides. On the other hand, the impact of the debris flow on the landslide is also not obvious.

(3) A susceptibility zoning map composed of two or more natural disasters is more comprehensive and significant, which provides valuable reference for researchers and engineering applications.

Data availability. The data used to support the findings of this study are included within the

article.

Author contributions. ZL was responsible for the writing and graphic production of the paper. CMW was responsible for the revision of the paper. DHM was responsible for calculation. KUJK was responsible for the translation.

Competing interests. The authors declare that they have no conflict of interest.

Special issue statement. This article is part of the special issue“Resilience to risks in built environments”. It is not associated with a conference.

Acknowledgements

This work was supported by Graduate Innovation Fund of Jilin University and the National Natural Science Foundation of China (Grant No. **41972267**, **41977221**, and **41572257**) .

References:

Alessandro Trigila, Carla Iadanza, Carlo Esposito, et al. Comparison of Logistic Regression and Random Forests techniques for shallow landslide susceptibility assessment in Giampilieri (NE Sicily, Italy). 2015, 249:119-136.

Ahmed Mohamed Youssef, Hamid Reza Pourghasemi, Zohre Sadat Pourtaghi, et al. Erratum to: Landslide susceptibility mapping using random forest, boosted regression tree, classification and regression tree, and general linear models and comparison of their performance at Wadi Tayyah Basin, Asir Region, Saudi Arabia. 2016, 13(5):1315-1318.

Anika Braun, Elias Leonardo Garcia Urquia, Rigoberto Moncada Lopez, et al. Landslide Susceptibility Mapping in Tegucigalpa, Honduras, Using Data Mining Methods. 2018.

Abdelaziz Merghadi, Ali P. Yunus, Jie Dou, Jim Whiteley, Binh ThaiPham,Dieu Tien Bui, Ram

387 Avtar and Boumezbeur Abderrahmane. Machine learning methods for landslide susceptibility
388 studies: A comparative overview of algorithm performance. 2020, 207
389 Breiman, L.,2001. Random Forests. Machine learning, 45(1): 5-32. doi:https://doi.org/10.1023/A:
390 10 1093340
391 Breiman L, Cutler A (2004) http://www.stat.berkeley.edu/users/Breiman/RandomForests/ccpapers.
392 H-Tml
393 Bui DT, Pradhan B, Lofman O, Revhaug I, Dick OB (2012) Landslide susceptibility assessment in
394 the Hoa Binh Province of Vietnam: a comparison of the Levenberg-Marquardt and Bayesian
395 regularized neural networks. Geomorphology. doi:10.1016/j.geomorph.2012.04.023
396 Bregoli F, Medina V, Chevalier G, Hürlimann M, Bateman A. Debris-flow susceptibility
397 assessment at regional scale: Validation on an alpine environment. Landslides.
398 2015;12(3):437-454. doi:10.1007/s10346-014-0493-x
399 Blais-Stevens A, Behnia P (2016) Debris flow susceptibility mapping using a qualitative heuristic
400 method and flow-R along the Yukon Alaska Highway Corridor, Canada. Nat Hazard Earth
401 Syst Sci 16(2):449–462.
402 Chung, C.F., Fabbri, A.G., 2003. Validation of spatial prediction models for landslide hazard
403 mapping. Nat. Hazards 30,451–472.
404 Carrara A, Crosta G, Frattini P (2008) Comparing models of debris-flow susceptibility in the
405 alpine environment. Geomorphology 94:353-378
406 Chunxiang Wang, Hideaki Marui, Gen Furuya, et al. Two Integrated Models Simulating Dynamic
407 Process of Landslide Using GIS. 2013.
408 Chung, C.F., Fabbri, A.G., 2003. Validation of spatial prediction models for landslide hazard

409 mapping. Nat. Hazards 30, 451–472.
410 Colkesen, I., Sahin, E.K., Kavzoglu, T., 2016. Susceptibility mapping of shallow landslides using
411 kernel-based Gaussian process, support vector machines and logistic regression. African
412 Earth Sciences]–>J. Afr. Earth Sci. 118, 53–64.
413 Chen, W., Xie, X., Wang, J., Pradhan, B., Hong, H., Bui, D.T., Duan, Z. and Ma, J., 2017. A
414 comparative study of logistic model tree, random forest, and classification and regression tree
415 models for spatial prediction of landslide susceptibility. Catena, 151, pp.147-160.
416 Cruden, D.M., Varnes, D.J., 1996. Landslide types and processes. In: Turner, A.K., Schuster, R.L.
417 (Eds.), Landslides, Investigation and Mitigation, Special Report 247. Transportation Research
418 Board, Washington D.C., pp. 36–75 ISSN: 0360-859X, ISBN: 030906208X.
419 Dai, F.C., Lee, C.F., 2002. Landslide characteristics and slope instability modelling using GIS,
420 Lantau Island, Hong Kong. Geomorphology 42, 213–228.
421 D. W. Park, N. V. Nikhil, S. R. Lee. Landslide and debris flow susceptibility zonation using
422 TRIGRS for the 2011 Seoul landslide event. 2013, 13(11):2833-2849.
423 Green, D.M., Swets, J.M., 1966. Signal Detection Theory and Psychophysics. John Wiley and
424 Sons, New York ISBN: 0-471-32420-5.
425 Guzzetti, F., Carrara, A., Cardinali, M., Reichenbach, P., 1999. Landslide hazard evaluation: a
426 review of current techniques and their application in a multi-scale study, Central Italy.
427 Geomorphology 31, 181–216.
428 Guzzetti, F., Galli, M., Reichenbach, P., Ardizzone, F., Cardinali, M., 2006a. Landslide hazard
429 assessment in the Collazzone area, Umbria, central Italy. Nat. Hazard. Earth Syst. Sci. 6,
430 115–131.

Guzzetti, F., Reichenbach, P., Ardizzone, F., Cardinali, M., Galli, M., 2006b. Estimating the quality of landslide susceptibility models. Geomorphology 81, 166–184.

Gomes, R. A. T., Guimaraes, R. F., Carvalho Júnior, O. A., Fernandes, N. F., and Amaral Jr., E. V.: Combining spatial models for shallow landslides and debris flows prediction, Remote Sens., 5,2219–2237, 2013

Hungr, O., Leroueil, S., Picarelli, L., 2013. The Varnes classification of landslide types, an update. Landslides 11 (2), 167–194.

Hurlimann M., Abanco C., Moya, J., Vilajosana I. 2013. Results and experiences gathered at the Rebaixader debris-flow monitoring site, Central Pyrenees, Spain. Landslides. doi:10.1007/s10346-013-0452-y 161-175

Huang Xiaohu, Guo Fei, Deng miaolin, Yi Wu, Huang Haifeng. 2019.Understanding the deformation mechanism and threshold reservoir level of the floating weight-reducing landslide in the Three Gorges Reservoir Area, China. Landslides DOI 10.1007/s10346-020-01435-1.

Haydar Y. Hussin, Veronica Zumpano, Paola Reichenbach, et al. Different landslide sampling strategies in a grid-based bi-variate statistical susceptibility model. 2016, 253:508-523.

Iverson,R.M., Reid,M.E., LaHusen,R.G.,1997. Debris-flow mobilization from landslides.Annual Review of Earth and Planetary Sciences 25,85–138.

Imaizumi F, Sidle RC, Tsuchiya S, Ohsaka O. 2006. Hydrogeomorphic processes in a steep debris flow initiation zone. Geophysical Research Letters 33: L10404.

James, G., Witten, D., Hastie, T., Tibshirani, R., 2013. An Introduction to Statistical Learning. Springer, New York, p. 441.

453 Lee, S., Dan, N.T., 2005. Probabilistic landslide susceptibility mapping on the Lai Chau province
454 of Vietnam: focus on the relationship between tectonic fractures and landslides.
455 Environmental Geology 48, 778–787.
456 Lan HX, Zhou CH, Wang LJ, Zhang HY, Li RH (2004) Landslide hazard spatial analysis and
457 prediction using GIS in the Xiao jiang watershed,Yunnan,China. Eng Geo l76:109–128
458 Linfeng Fan, Peter Lehmann, Brian McArdell, et al. Linking rainfall-induced landslides with
459 debris flows runout patterns towards catchment scale hazard assessment. 2017, 280:1-15.
460 Liqiang Tong, Wensheng Qi, Guoying An,Chunling Liu. Remote sensing survey of major
461 geological disasters in the Himalayas[J].Journal of engineering geology,2019,27(03):496.
462 Melton M A． The Geomorphic and Paleoclimatic Significance of Alluvial Deposits in Southern
463 Arizona: A Reply［J］. The Journal of Geology，1965，73(1) : 102 －106．
464 Mariantonietta Ciurleo, Leonardo Cascini, Michele Calvello. A comparison of statistical and
465 deterministic methods for shallow landslide susceptibility zoning in clayey soils. 2017,
466 223:71-81.
467 Maria Giuseppina Persichillo, Massimiliano Bordoni, Claudia Meisina, et al. Shallow landslides
468 susceptibility assessment in different environments. 2017, 8(2):748-771.
469 Ma C., Deng J., Wang R. Analysis of the triggering conditions and erosion of a run off triggered
470 debris flow in Mi yun County, Beijing, China. Landslide, 2018, DOI
471 10.1007/s10346-018-1080-3
472 P. Aleotti, R. Chowdhury. Landslide hazard assessment: summary review and new perspectives.
473 1999, 58(1):21-44.
474 Pradhan, B., 2010. Landslide susceptibility mapping of a catchment area using frequency ratio,

475 fuzzy logic and multivariate logistic regression approaches. J. Indian Soc. Remote Sens. 38
476 (2), 301–320.
477 Pedregosa,F., Varoquaux,G., Gramfort, A., et al., 2011. Scikit-Learn: Machine Learning in Python.
478 Journal of machine learning research, 12(10): 2825-2830.
479 P. Vorpahl, H. Elsenbeer, M. Märker, and B. Schröder, “How can statistical models help to
480 determine driving factors of landslides?” Ecol. Model., vol. 239, pp. 27–39, 2012
481 Pourghasemi HR, Moradi HR, Fatemi Aghda SM (2013a) Landslide susceptibility mapping by
482 binary logistic regression, analytical hierarchy process, and statistical index models and
483 assessment of their performances. Nat Hazards 69:749–779. doi:10.1007/s11069-013-0728-5
484 Pourghasemi HR, Pradhan B, Gokceoglu C, Mohammadi M, Moradi HR (2013b) Application of
485 weights-of-evidence and certainty factor models and their comparison in landslide
486 susceptibility mapping at Haraz watershed, Iran. Arab J Geosci 6(7):2351–2365.
487 doi:10.1007/s12517-012-0532-7
488 Reichenbach,P.,Rossi,M.,Malamud,B.D.,et al.,2018.A Review of Statistically-Based Landslide
489 Susceptibility Models. Earth-Science Reviews, 180(5): 60-91.
490 doi:https://doi.org/10.1016/j.earscirev. 2018. 03. 001
491 Simoni A., Bernard, M., Berti M., BoreggioM., Lanzoni S., Stancanelli L., Gregoretti C (2020)
492 Runoff-generated debris flows: observation of initiation conditions and erosion-deposition
493 dynamics along the channel at Cancia (eastern Italian Alps). Earth Surface Processes and
494 Landforms -doi:10.1002/esp.4981
495 Shou-Hao Chiang, Kang-Tsung Chang, Alessandro C. Mondini, et al. Simulation of event-based
496 landslides and debris flows at watershed level. 2011, 138(1):306-318.

497 Takahashi, T., 1978. Mechanical characteristics of debris flow. Journal of the Hydraulics Division
498 104, 1153–1169.
499 Theule, J.I., Liebault, F., Loye, A., Laigle, D., and Jaboyedoff, M., 2012. Sediment budget
500 monitoring of debris flow and bedload transport in the Manival Torrent, SE France.
501 Teigila A, et al. Comparison of Logistic Regression and Random Forests techniques for shallow
502 landslide susceptibility assessment in Giampilieri (NE Sicily, Italy)][J]. Geomorphology
503 Science Letter, 2015
504 Taskin Kavzoglu, Emrehan Kutlug Sahin, Ismail Colkesen, Selecting optimal conditioning factors
505 in shallow translational landslide susceptibility mapping using genetic algorithm,Engineering
506 Geology,Volume192, 2015, Pages 101-112.
507 Varnes DJ (1978) Slope movement types and processes, in Schuster, R.L., and Krizek, R.J., eds.,
508 Landslides: Analysis and control, National Research Council, Washington, D.C.,
509 Transportation Re- search Board, National Academy Press, Special Report 176, p. 11–33
510 Varnes, D.J., IAEG Commission on Landslides and other Mass-Movements, 1984. Landslide
511 Hazard Zonation: A Review of Principles and Practice. The UNESCO Press, Paris (63 pp).
512 van Westen CJ, Castellanos E, Kuriakose SL (2008) Spatial data for landslide susceptibility,
513 hazard, and vulnerability assessment: an overview. Eng Geol 102(3–4):112–131
514 Wilson JP, Gallant JC (2000) Digital terrain analysis. In: Wilson JP, Gallant JC (eds) Terrain
515 analysis. John Wiley & Sons, New York, pp 1–27
516 Yilmaz, I., 2010. The effect of the sampling strategies on the landslide susceptibility mapping by
517 conditional probability and artificial neural networks. Environ. Earth Sci. 60,505–519.
518 Zhang, K., Wu, X., Niu, R., Yang, K. and Zhao, L., 2017. The assessment of landslide

519 susceptibility mapping using random forest and decision tree methods in the Three Gorges
520 Reservoir area, China. Environmental Earth Sciences, 76(11), pp.1-20.
521 Zhou, W., Fan.J., Tang, C., Yang, G. (2019)Empirical relationships for the estimation of debris
522 flow runout distances on depositional fans in the Wenchuan earthquake zone. Journal of
523 Hydrology, 577, https://doi.org/10.1016/j. jhydrol. 2019. 123932
524 Zhu Liang, Changming Wang, , Zhi-Min Zhang and Kaleem-Ullah-Jan Khan. A comparison of
525 statistical and machine learning methods for debris flow susceptibility mapping. Stoch
526 Environ Res Risk Assess (2020a) https://doi.org/10.1007/s00477-020-01851-8
527 Zhu Liang, Changming Wang, Songling Han, Kaleem Ullah Jan Khan, and Yiao Liu.
528 Classification and susceptibility assessment of debris flow based on a semi-quantitative
529 method combination of the fuzzy C-means algorithm, factor analysis and efficacy
530 coefficient.Nat. Hazards Earth Syst. Sci., 20, 1287–1304, 2020b
531 https://doi.org/10.5194/nhess-20-1287-2020
532 Zhu Liang, Wang Changming and Kaleem-Ullah-Jan Khan. Application and comparison of
533 different ensemble learning machines combining with a novel sampling strategy for shallow
534 landslide susceptibility mapping. Stoch Environ Res Risk Assess (2020c).
535 https://doi.org/10.1007/s00477-020-01893-y

536 **Table 1** Models' performance using training dataset

Metrics	Landslide	Debris flow
TP（%）	88.71	87.80
TN（%）	91.89	88.89
FP（%）	11.29	12.20

FN（%）	8.11	11.11
Sensitivity（%）	91.62	88.77
Specificity（%）	89.06	87.93
Accuracy（%）	90.65	88.57
AUC	0.976	0.967

537 **Table 2** Models' performance using verification dataset

Metrics	Landslide	Debris flow
TP（%）	85.56	85.71
TN（%）	89.09	84.62
FP（%）	14.44	14.29
FN（%）	10.91	15.38
Sensitivity（%）	88.69	84.79
Specificity（%）	86.05	85.55
Accuracy（%）	87.33	85.17
AUC	0.902	0.892

538 **Table 3** Variables importance assigned for landslide

Test group	Slope angle	Distance to fault	Plan curvature	Topographic wetness index	Distance to road	Maximum elevation difference	Profile curvature	Elevation
Landslide	0.21	0.19	0.17	0.13	0.08	0.07	0.06	0.05

539 **Table 4** Variables importance assigned for debris flow

Test group	Main channel length	Roundness	Slope angle	Elevation	Maximum elevation difference	Melton	Basin area
Debris flow	0.25	0.16	0.14	0.13	0.12	0.1	0.1

Table 5 The overlap number of debris flow and landslide height and very high-class mapping units

Debris flow \ Landslide	Very low	Low	High	Very high
High	3/23	1/23	5/23	12/23
Very high	2/26	2/26	8/26	11/26

Table 6 Statistical parameters of the two models

Statistical parameters \ Model	Model 1	Mode 2
KMO	0.766	0.643
Sig.	0.001	0.003

Table 7 The correlation coefficients between common factors and primitive variables

Factor	F1	F2	F3
NDVI	0.386	-0.336	-0.621
Basin area	0.897	-0.007	0.041
Main channel length	0.984	0.046	-0.023
Slop angle	-0.223	0.829	0.455
Maximum elevation difference	0.744	0.66	0.011
Rainfall	-0.768	0.33	0.201
Average gradient of main channel	-0.753	0.544	0.106

Drainage density	-0.844	0.06	0.015
Roundness	0.331	0.14	0.818
Elevation	0.133	0.846	0.382
Distance to fault	-0.16	0.211	0.421
Melton	-0.625	0.737	0.149
Contribution rate (%)	41.2	24.7	16.7
Accumulative contribution (%)	41.2	65.9	83.6

543 **Table 8** The correlation coefficients between common factors and primitive variables

Factor	C1	C2	C3	C4
NDVI	0.042	-0.079	-0.279	-0.813
Basin area	0.802	-0.344	0.057	0.009
Main channel length	0.885	0.126	-0.196	0.227
Slop angle	0.009	0.748	0.58	-0.057
Maximum elevation difference	0.801	0.434	-0.128	0.144
Rainfall	0.197	-0.076	-0.487	0.637
Average gradient of main channel	-0.744	0.205	0.15	-0.23
Drainage density	-0.776	-0.176	-0.267	0.117
Roundness	-0.014	0.022	0.896	-0.002
Elevation	0.34	0.746	0.25	0.326
Distance to fault	0.31	0.289	-0.344	0.757
Melton	-0.182	0.932	-0.192	0.061

Contribution rate (%)	29.2	20.3	15.2	15.8
Accumulative contribution (%)	29.2	49.5	64.7	80.5

544 **Table 9** The overlap number of landslide and debris flow height and very-high class mapping units

Landslide \ Debris flow	Very low	Low	High	Very high
High	36/167	33/167	25/167	43/167
Very high	48/179	40/179	25/179	28/179

545 **Table 10** Comprehensive evaluation of landslide-debris flow susceptibility

Landslide \ Debris flow	Low or Very low	High or Very high
Low or Very low	Low	Moderate
High or Very high	Moderate	High

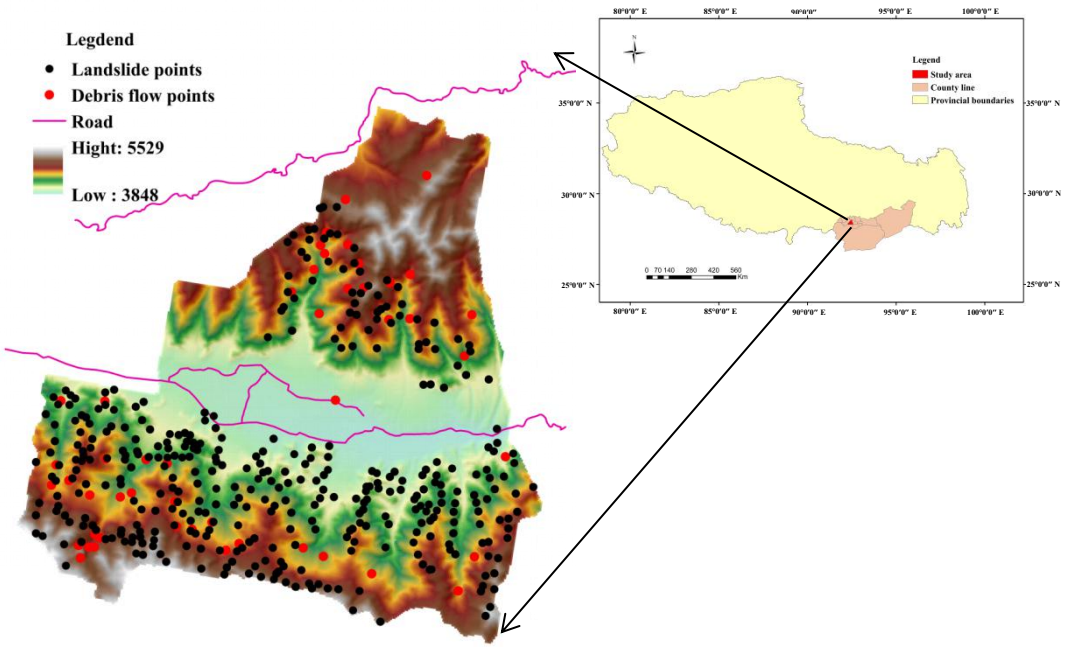

546

547 **Fig.1.** Location map of the study area showing landslide and debris flow inventory.

548

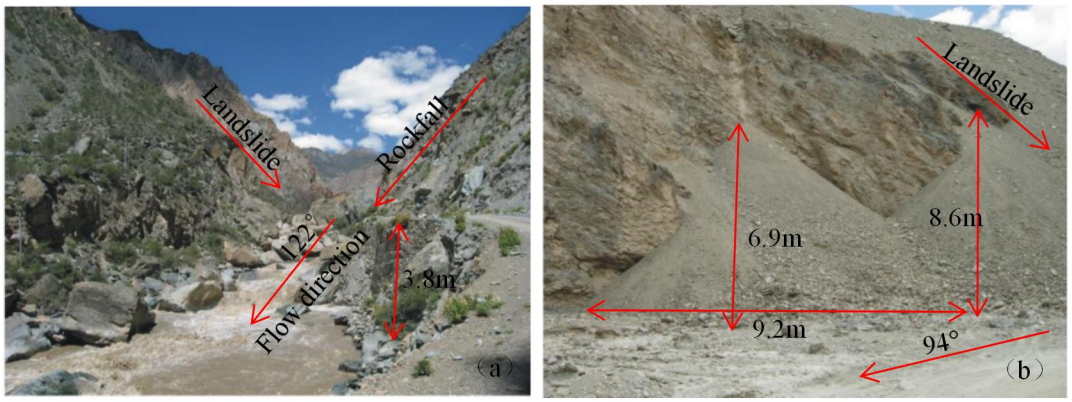

549

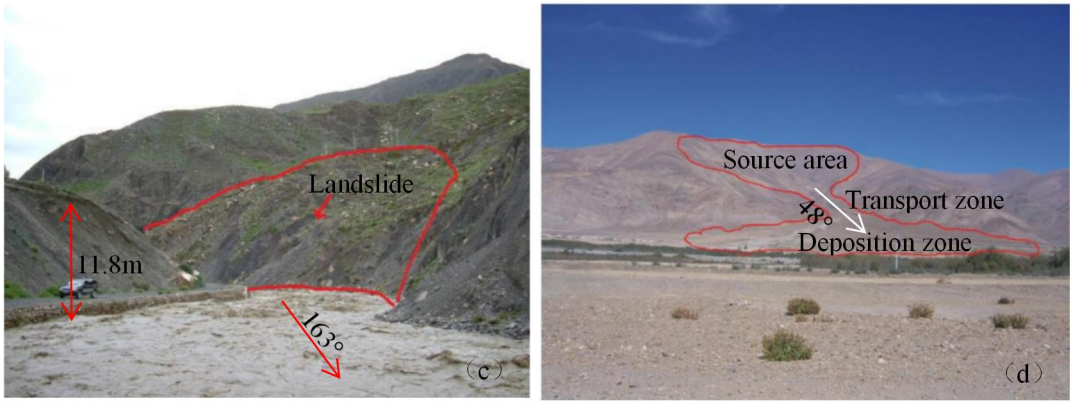

550 **Fig.2.** Photos of landslide or debris flow: **(a)** Lunba landslide in a tributary; **(b)** Zhenqiong landslide in

551 Jiayu village; **(c)** Debris flow in Misha Township; **(d)** Debris flow in Lelong Village.

552

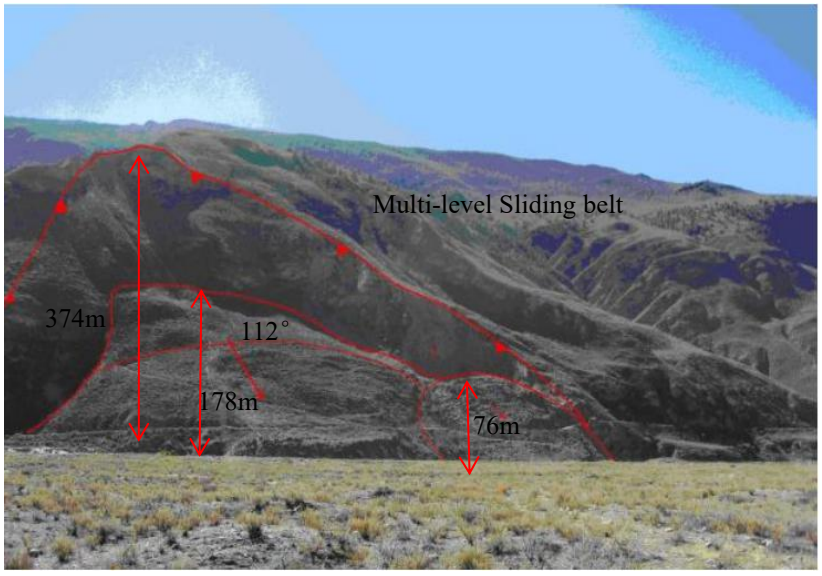

553 **Fig.3.** Multistage landslide in Xiongqu village

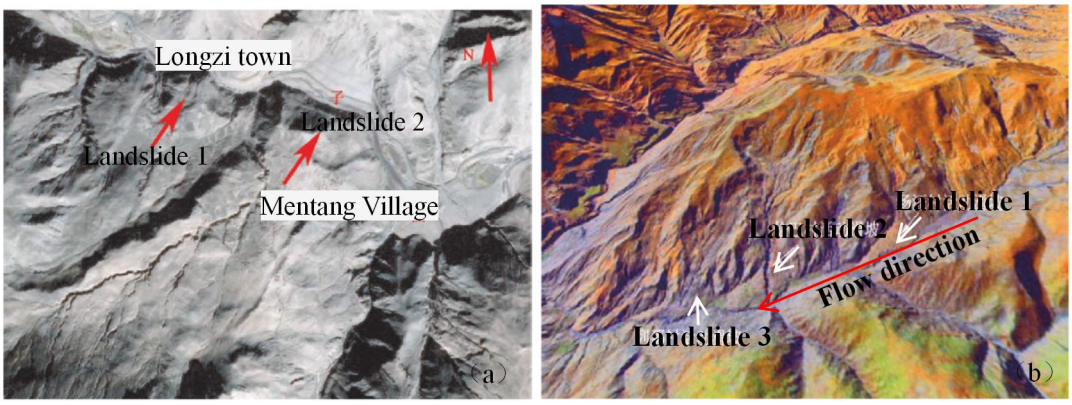

554

555 **Fig.4.** Stereo remote sensing map of landslides in Longzi Township (Tong et al., 2019):（**a**）Landslides

556 in Longzi town; **(b)** Landslides in Malu town.

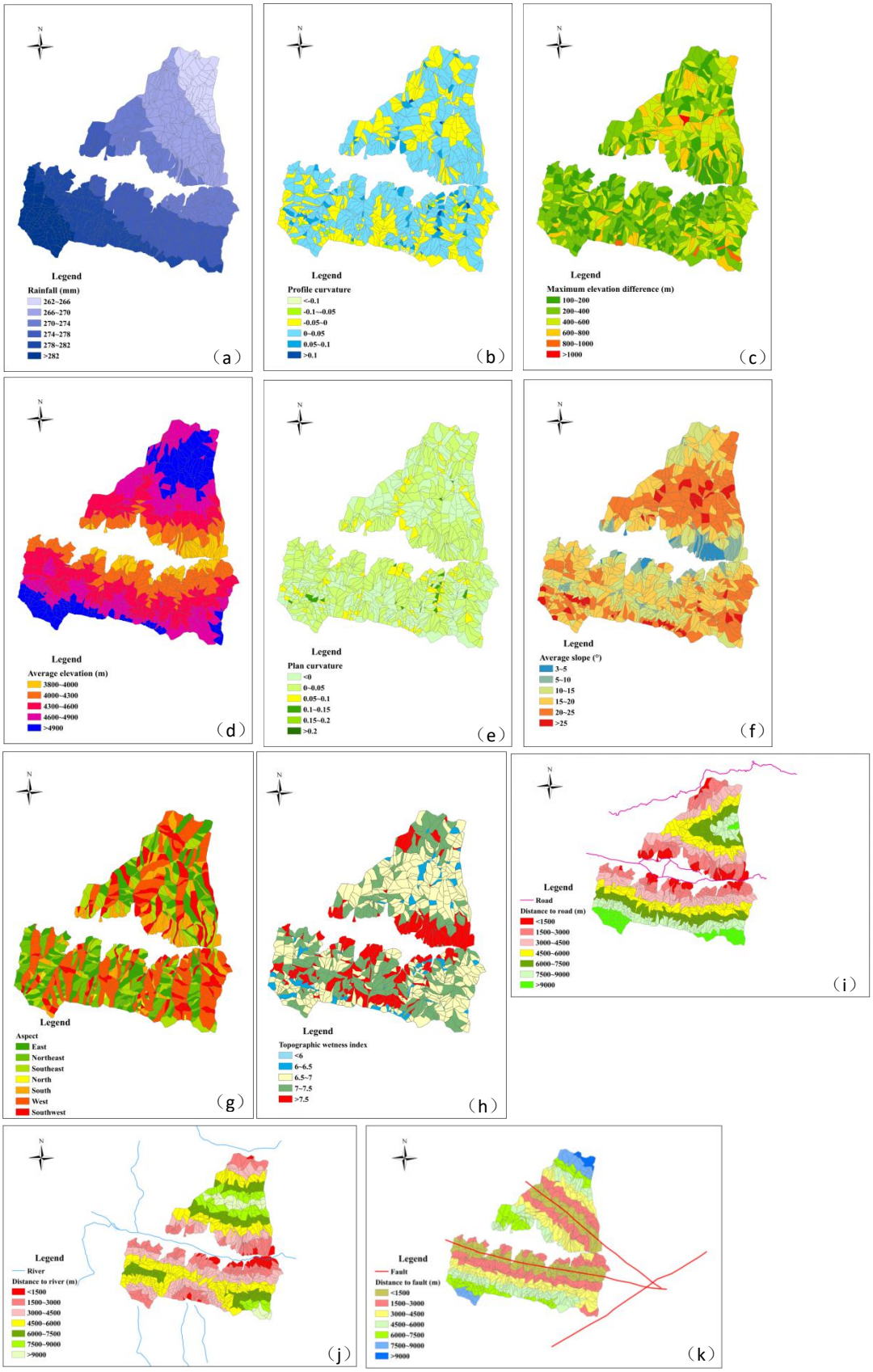

Fig.5. Study area thematic maps for landslide: (**a**) Rainfall; (**b**) Profile curvature; (**c**) Maximum elevation difference; (**d**) Average elevation; (**e**) Plan curvature; (**f**) Average slope; (**g**) Aspect;

（**h**）Wetness;（**i**）Distance to road;（**j**）Distance to river;（**k**）Distance to fault.

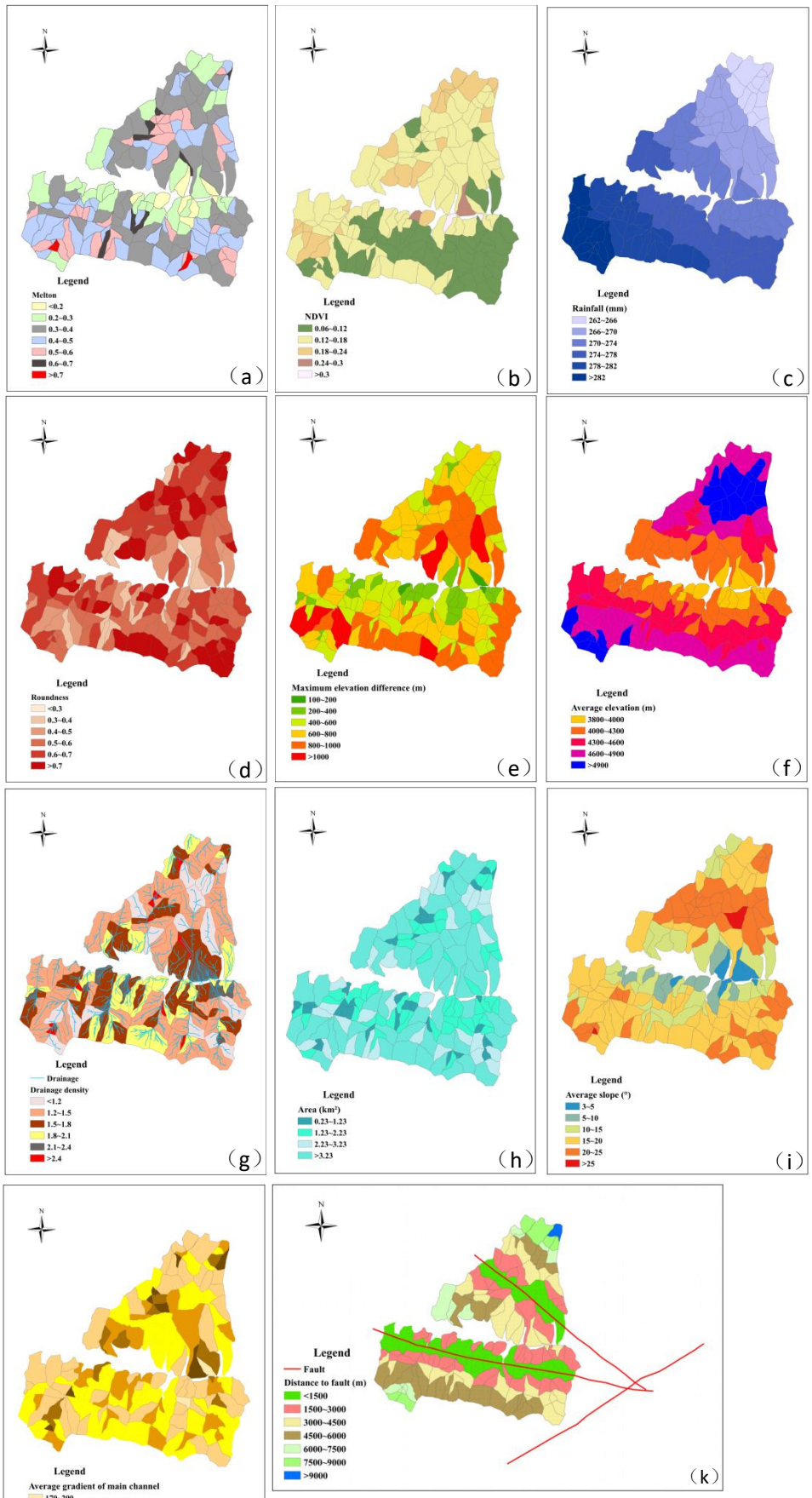
Legend
Melton
<0.2
0.2~0.3
0.3~0.4
0.4~0.5
0.5~0.6
0.6~0.7
>0.7
(a)
Legend
NDVI
0.06~0.12
0.12~0.18
0.18~0.24
0.24~0.3
>0.3
(b)
Legend
Rainfall (mm)
262~266
266~270
270~274
274~278
278~282
>282
(c)
Legend
Roundness
<0.3
0.3~0.4
0.4~0.5
0.5~0.6
0.6~0.7
>0.7
(d)
Legend
Maximum elevation difference (m)
100~200
200~400
400~600
600~800
800~1000
>1000
(e)
Legend
Average elevation (m)
3800~4000
4000~4300
4300~4600
4600~4900
>4900
(f)
Legend
Drainage
Drainage density
<1.2
1.2~1.5
1.5~1.8
1.8~2.1
2.1~2.4
>2.4
(g)
Legend
Area (km²)
0.23~1.23
1.23~2.23
2.23~3.23
>3.23
(h)
Legend
Average slope (°)
3~5
5~10
10~15
15~20
20~25
>25
(i)
Legend
Average gradient of main channel
170~200
200~400
400~600
600~800
800~1000
>1000
(j)
Legend
Fault
Distance to fault (m)
<1500
1500~3000
3000~4500
4500~6000
6000~7500
7500~9000
>9000
(k)

561

562 **Fig.6.** Study area thematic maps for debris flow: （**a**）Melton; （**b**）NDVI; （**c**）Rainfall; （**d**）Roundness;

563 （**e**）Maximum elevation difference; （**f**）Average elevation; （**g**）Drainage density; （**h**）Area; （**i**）

564 Average slope; （**j**）Average gradient of main channel; （**k**）Distance to fault.

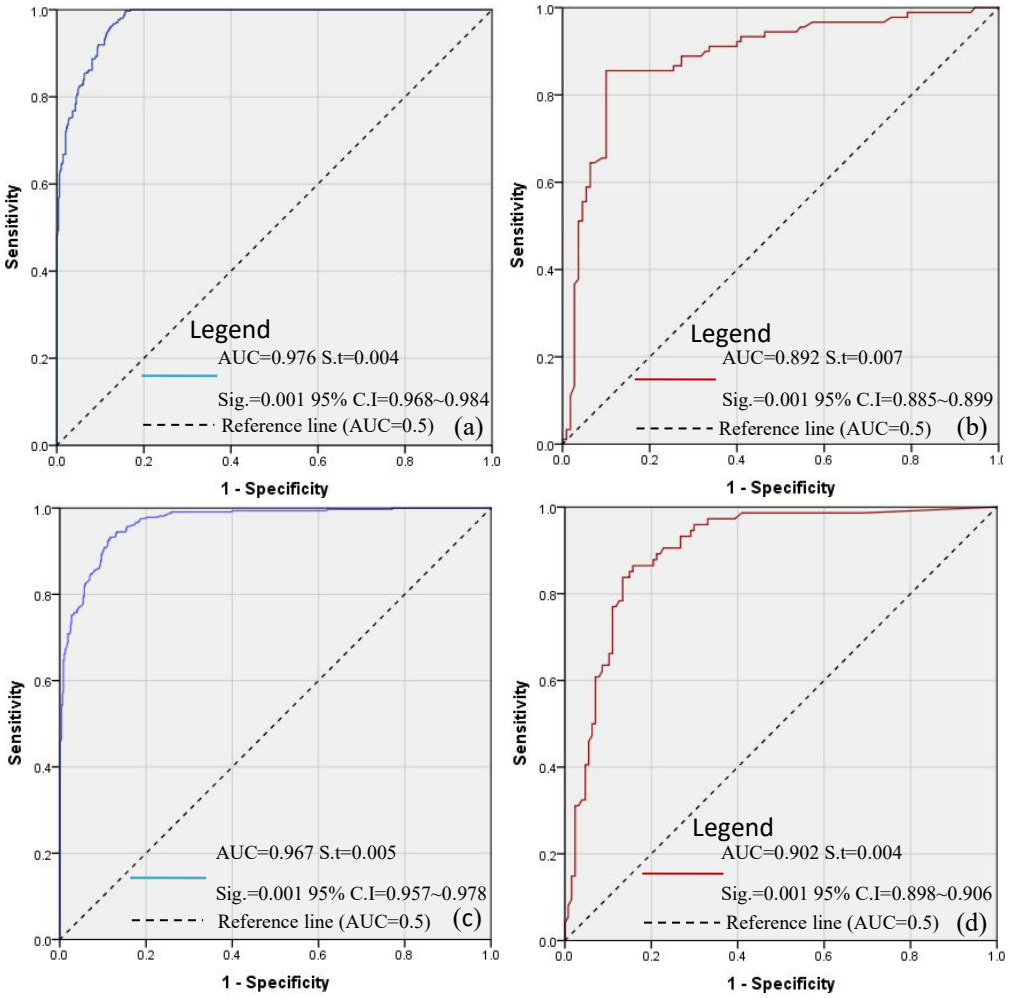

565

566 **Fig. 7.** Analysis of ROC curve for the two susceptibility maps: **(a)** Success rate curve of landslide using

567 the training dataset; **(b)** Prediction rate curve of landslide using the validation dataset; **(c)** Success rate

568 curve of debris flow using the training dataset; **(d)** Prediction rate curve of debris flow using the

569 validation dataset.

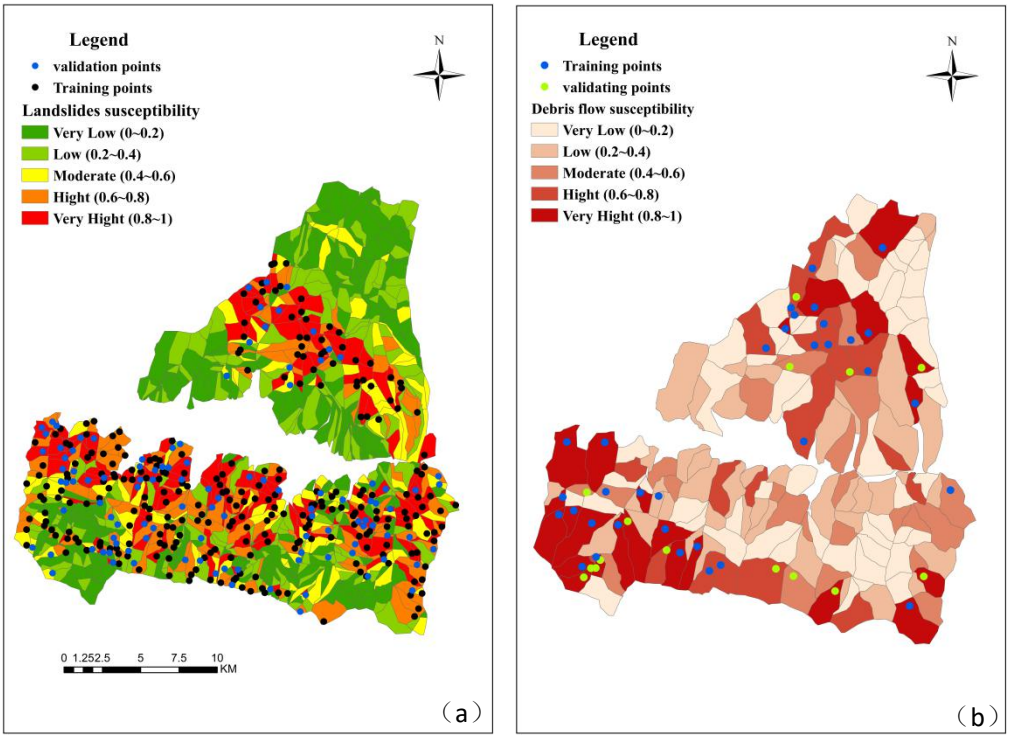

570

571 **Fig.8.** Susceptibility maps: （**a**） Landslide susceptibility zoning map; （**b**） Debris flow susceptibility

572 zoning map.

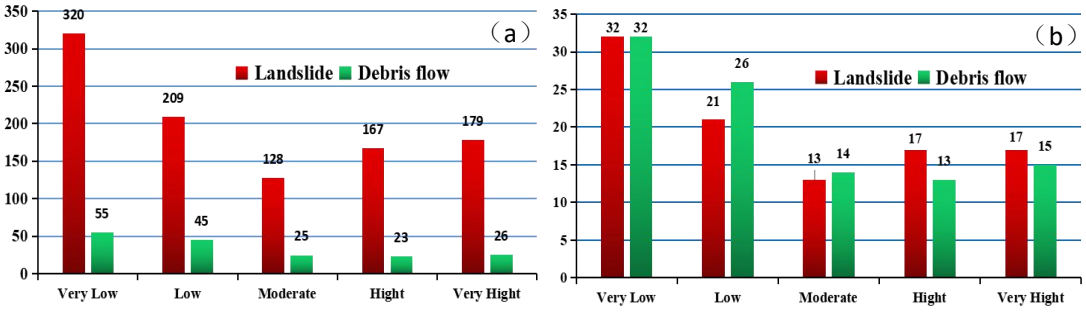

573

574 **Fig. 9.** Numbers and percentage of units in different susceptibility classes for landslide and debris flow:

575 **(a)** Numbers of units in different susceptibility classes for landslide and debris flow; **(b)** Percentages of

576 different susceptibility classes for landslide and debris flow.

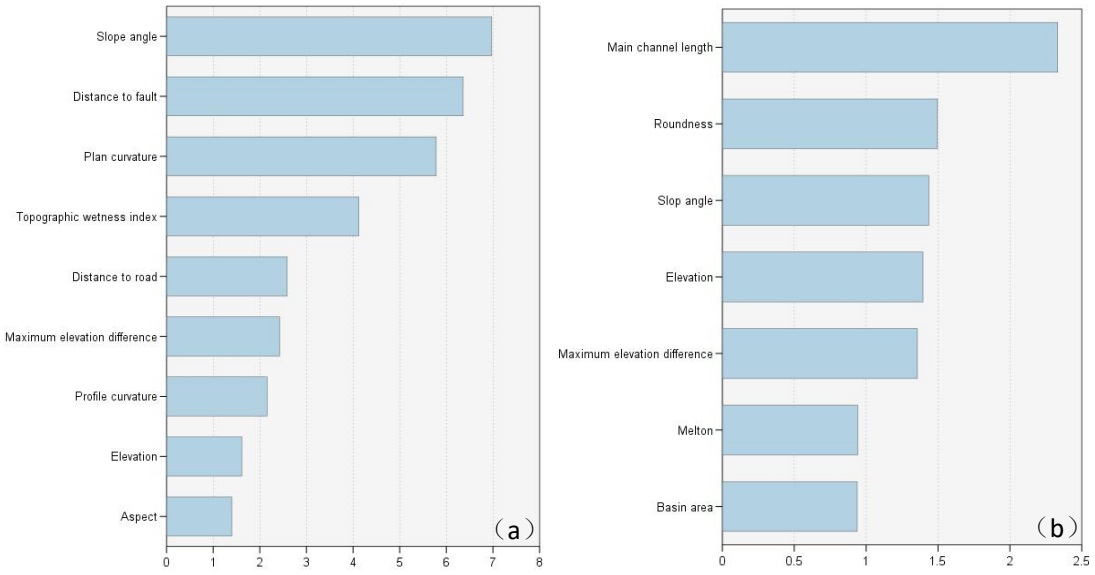

577

578 **Fig.10.** Parametric importance graphics obtained from RF model: **(a)** Parametric importance graphics

579 of landslide; **(b)** Parametric importance graphics of debris flow.

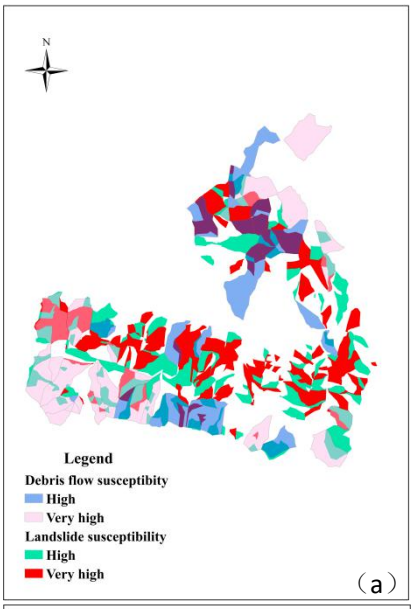
N
Legend
Debris flow susceptibity
High
Very high
Landslide susceptibility
High
Very high
(a)

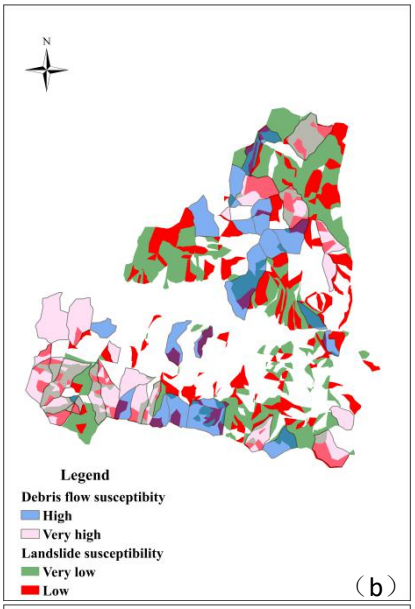
N
Legend
Debris flow susceptibity
High
Very high
Landslide susceptibility
Very low
Low
(b)

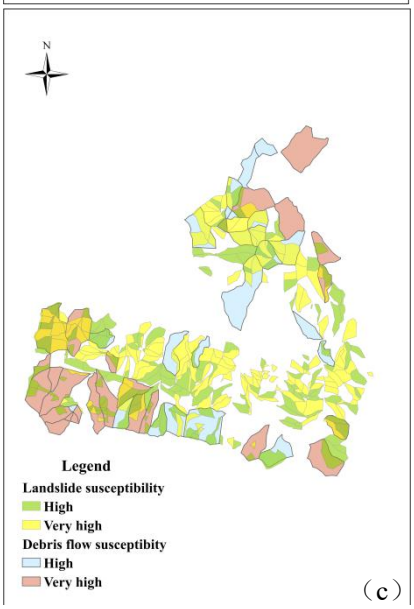
N
Legend
Landslide susceptibility
High
Very high
Debris flow susceptibity
High
Very high
(c)

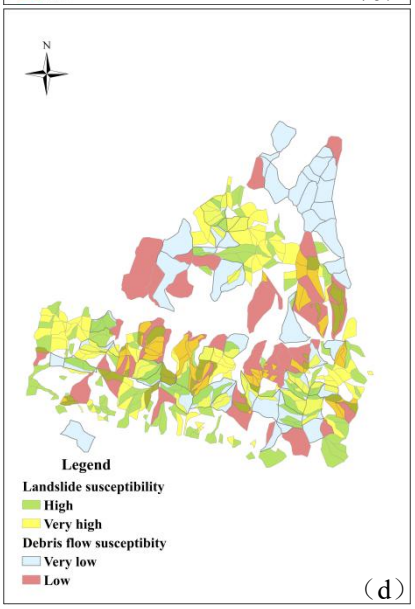
N
Legend
Landslide susceptibility
High
Very high
Debris flow susceptibity
Very low
Low
(d)

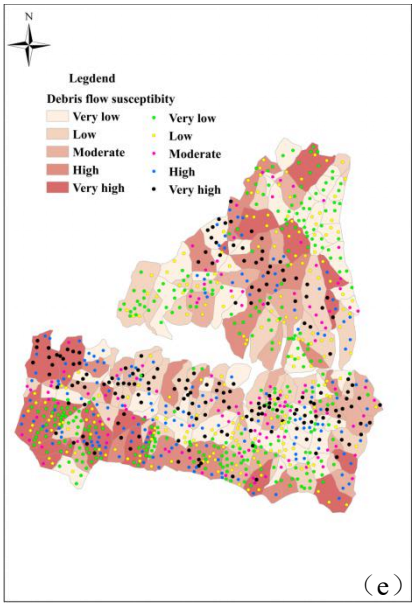
N
Legdend
Debris flow susceptibity
Very low
Low
Moderate
High
Very high
Very low
Low
Moderate
High
Very high
(e)

580

581 **Fig.11.** Landslide-debris flow susceptibility maps: **(a)** Height and very high-class watershed units with
582 high or very high slope units; **(b)** High or very high-class watershed units with low or very low slope
583 units; **(c)** High or very high-class slope units with high or very high-class watershed units; **(d)** Mapping
584 units.
585
586
587
588